NASA TECHNICAL NOTE

NASA TN D-2970

NASA TN D-2970

A DESCRIPTION OF NUMERICAL METHODS AND COMPUTER PROGRAMS FOR TWO-DIMENSIONAL AND AXISYMMETRIC SUPERSONIC FLOW OVER BLUNT-NOSED AND FLARED BODIES

by Mamoru Inouye, John V. Rakich, and Harvard Lomax

Ames Research Center
Moffett Field, Calif.

NATIONAL AERONAUTICS AND SPACE ADMINISTRATION • WASHINGTON, D. C. • AUGUST 1965

A DESCRIPTION OF NUMERICAL METHODS AND COMPUTER PROGRAMS FOR TWO-DIMENSIONAL AND AXISYMMETRIC SUPERSONIC FLOW OVER BLUNT-NOSED AND FLARED BODIES

By Mamoru Inouye, John V. Rakich,
and Harvard Lomax

Ames Research Center
Moffett Field, Calif.

NATIONAL AERONAUTICS AND SPACE ADMINISTRATION

For sale by the Clearinghouse for Federal Scientific and Technical Information
Springfield, Virginia 22151 – Price $2.00

A DESCRIPTION OF NUMERICAL METHODS AND COMPUTER PROGRAMS FOR TWO-DIMENSIONAL AND AXISYMMETRIC SUPERSONIC FLOW OVER BLUNT-NOSED AND FLARED BODIES

By Mamoru Inouye, John V. Rakich, and Harvard Lomax
Ames Research Center

SUMMARY

The computer programs developed at Ames Research Center for calculating the inviscid flow field around blunt-nosed bodies are described briefly and their application to specific shapes is demonstrated. The programs solve numerically the exact equations of motion for plane or axisymmetric bodies at zero angle of attack and for a perfect gas or a real gas in thermodynamic equilibrium. An inverse method is used for the subsonic-transonic region, and the method of characteristics is used for the supersonic region. Results are shown for several body shapes in both perfect and real gas flow, including a comparison between air and a CO_2-N_2 mixture. Presented are shock-wave shapes and distributions of pressure and other flow variables along the body and across the shock layer.

INTRODUCTION

Aircraft and spacecraft designers are faced with the problem of determining the inviscid flow field over blunt-nosed bodies for supersonic flight at speeds encompassing those attained in planetary entry. In addition to the blunt nose, a typical body shape may have a flared afterbody which further complicates the problem. The dominant features of such a flow field are indicated in sketch (a). There occurs a detached bow wave that is normal at the

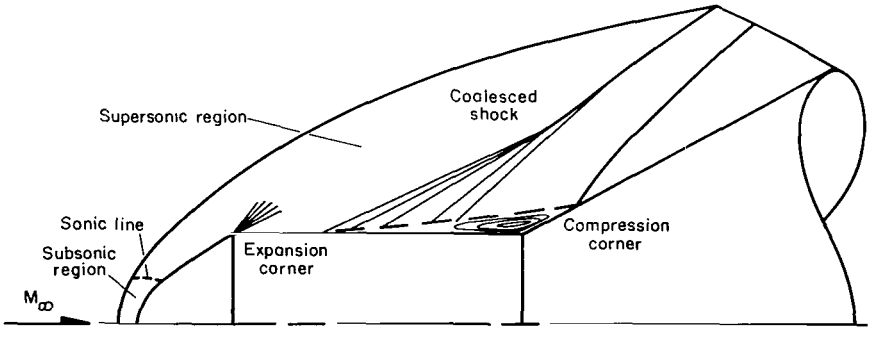

Typical flow field

Sketch (a)

axis of symmetry and decays in strength as it approaches a Mach wave at large distances from the body. The flow behind the shock wave is subsonic in the nose region bounded by the sonic line and becomes supersonic over the afterbody. Expansion waves and embedded shocks may occur as a result of corners. In addition, an embedded shock may arise from coalescence of compression waves from the surface or from separation of the boundary layer, which often occurs on this type of body. Analysis of the viscous region is beyond the scope of the present study; however, its study depends on a knowledge of the external inviscid flow.

A number of exact and approximate techniques for determining the flow field depicted in sketch (a) have been reported. Some of the more recent contributions are references 1 through 4 for blunt-body flows, and references 5 and 6 for the supersonic region downstream of the nose. For flared bodies, exact numerical results have been reported in reference 7 while approximate methods may be found in references 8 through 10. Hayes and Probstein (ref. 11) present a more complete discussion of the entire flow field.

The computer programs that are described in the present report solve numerically the exact equations of motion for plane and axisymmetric flow at zero angle of attack and provide the complete inviscid flow field between the body and the shock wave. The fluid may be a perfect gas or a real gas in thermodynamic equilibrium. An inverse method (ref. 3) is used for the subsonic-transonic region (referred to as the blunt-body program), and the method of characteristics (ref. 5) is used to extend the calculations downstream in the supersonic region. These computer programs were written in FORTRAN II for use on an IBM 7094 at Ames Research Center, but have been made available to a number of other organizations. The distribution of these programs has created a need for a more complete description and documentation than is presently available. The present report is intended to partially fulfill this need.

The purpose of the present report is to provide a general description of the Ames flow-field computer programs and to present results of calculations that demonstrate the range of applicability. The governing equations of motion are introduced briefly at the start. Then the methods used to solve the equations are presented. No attempt is made to provide a complete listing of all the subroutines and flow charts. Instead, detailed descriptions are provided only for selected portions of the programs that warrant special consideration. The information contained in this report should acquaint the reader with the general logic followed in the programs and be helpful in diagnosing small difficulties or in making minor modifications.

Sample results are presented for shock-wave shape, surface-pressure distribution, and shock-layer profiles of total pressure, static pressure, density, and velocity for various free-stream conditions and body shapes. The first examples demonstrate how a simple modification improves the accuracy of the calculations in regions with large entropy (or vorticity) gradients. Then comparisons are made with flow-field results obtained by means of an integral method for the blunt-body solution. Comparisons are also made with experimental results obtained for a body with a flare. Finally, examples of calculations for real gases in thermodynamic equilibrium are presented.

SYMBOLS

a	speed of sound
B_b	ellipsoid bluntness, $(b/c)^2$
b,c	semiaxes of ellipsoid
h	enthalpy
h_t	total enthalpy
M	Mach number
n	coordinate normal to a streamline
p	static pressure
p_t	total pressure
R	nose or cylinder radius
S	entropy
s,t	sheared coordinates (see eqs. (8))
u,v	velocity components in x,y directions
V	velocity
X	shock-wave shape
x,y	cylindrical coordinates with origin at body nose
γ	ratio of specific heats
Δ	shock standoff distance
δ	angle of corner on the body
ϵ	index for number of degrees of symmetry; $\epsilon = 0$ for plane symmetric flow, and $\epsilon = 1$ for axisymmetric flow
θ	flow angle
θ_c	cone angle
μ	Mach angle

ρ density

ψ stream function

Subscripts

b body

s shock

∞ free-stream conditions

EQUATIONS

The partial differential equations that must be satisfied for steady, inviscid flow are as follows:

Continuity of mass

$$\frac{\partial}{\partial x}\left(\rho u y^{\epsilon}\right) + \frac{\partial}{\partial y}\left(\rho v y^{\epsilon}\right) = 0 \tag{1}$$

where $\epsilon = 0$ for plane symmetric flow and $\epsilon = 1$ for axisymmetric flow.

Momentum equations

x direction

$$\rho u \frac{\partial u}{\partial x} + \rho v \frac{\partial u}{\partial y} + \frac{\partial p}{\partial x} = 0 \tag{2}$$

y direction

$$\rho u \frac{\partial v}{\partial x} + \rho v \frac{\partial v}{\partial y} + \frac{\partial p}{\partial y} = 0 \tag{3}$$

Energy equation

$$u \frac{\partial p}{\partial x} + v \frac{\partial p}{\partial y} - a^2\left(u \frac{\partial \rho}{\partial x} + v \frac{\partial \rho}{\partial y}\right) = 0 \tag{4}$$

where a is the isentropic speed of sound defined by

$$a^2 = \left(\frac{\partial p}{\partial \rho}\right)_S \tag{5}$$

To solve these equations for a given set of boundary conditions, the thermodynamic properties of the gas are required; for example,

$$a^2 = f(p,\rho) \tag{6}$$

For a perfect gas these relationships are merely functions of the gas constant and ratio of specific heats. For example, equation (6) becomes

$$a^2 = \frac{\gamma p}{\rho} \tag{7}$$

For a real gas the equilibrium composition and thermodynamic properties must be obtained by means of statistical mechanics. These calculations can be done independently of the flow-field equations, and the results can be tabulated for later use. Dr. Harry E. Bailey of Ames Research Center has recently performed these calculations for various gas mixtures of current interest following the assumptions and approximations made by Marrone (ref. 12). The data cover temperatures to 25,000° K in 250° increments and densities from 10^{-7} to 10^{3} times a reference density, ρ_o, which is the density of the mixture for a temperature of 273.16° K and a pressure of 0.101325 MN/m^2 (1 atmosphere). For example, the properties for carbon dioxide are reported in reference 13.

The thermodynamic properties in this form are not suitable for optimal use in a computer program. Some approximations are necessary to minimize the computing time and storage requirements. For use in the present programs, the calculated values of the properties have been spline fitted with cubics by the method of reference 14, and the coefficients of the cubics have been stored on magnetic tape. A special subroutine reads the tape, searches for the proper coefficients, and evaluates the desired properties. This approximate technique, in general, yields results within 1 percent of the original data. At present the thermodynamic properties for air and the twelve mixtures of nitrogen, carbon dioxide, and argon listed in table I are available on tape.

For moderate temperatures, for example, below about 2000° K for air, dissociation and ionization can be neglected, and the imperfect gas effects are due to the excitation of the vibrational states. The thermodynamic properties for such thermally perfect gases have been calculated in reference 15 and have also been stored on tape for use in the present programs.

The system of equations is now complete. In general, the four partial differential equations (eqs. (1) through (4)) must be solved simultaneously for the four dependent variables p,ρ,u, and v. In the following sections the methods used to solve these equations numerically in the subsonic-transonic region and in the supersonic region are discussed.

METHOD OF SOLUTION FOR SUBSONIC-TRANSONIC REGION

In the nose region of blunt bodies, equations (1) through (4) exhibit different character; namely, the equations are elliptic in the subsonic region,

parabolic on the sonic line, and hyperbolic in the supersonic region. Despite these complications, an inverse method (see, e.g., ref. 1) has been found effectual for solving such flow fields. In the application of this method, a shock shape is assumed and the equations are integrated numerically by a finite-difference method to determine the corresponding body shape. The particular version used in this report is reported in detail in reference 3; hence, only a brief description will follow.

Since the initial boundary conditions are specified along the shock, a sheared, nonorthogonal coordinate system with one axis coincident with the shock is useful (see sketch (b)). The new coordinates are defined as follows:

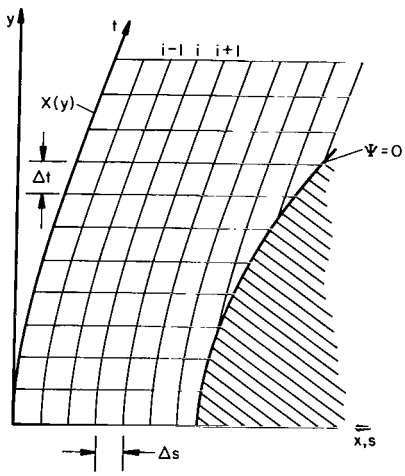

Sketch (b)

$$\left.\begin{aligned} s &= x - X(y) \\ t &= y \end{aligned}\right\} \tag{8}$$

Equations (1) through (4) are then transformed and expressed in the following form:

$$\left.\begin{aligned} \frac{\partial p}{\partial s} &= \varphi_1\left(t,p,\rho,u,v,\frac{\partial p}{\partial t},\frac{\partial \rho}{\partial t},\frac{\partial u}{\partial t},\frac{\partial v}{\partial t}\right) \\ \frac{\partial \rho}{\partial s} &= \varphi_2\left(t,p,\rho,u,v,\frac{\partial p}{\partial t},\frac{\partial \rho}{\partial t},\frac{\partial u}{\partial t},\frac{\partial v}{\partial t}\right) \\ \frac{\partial u}{\partial s} &= \varphi_3\left(t,p,\rho,u,v,\frac{\partial p}{\partial t},\frac{\partial \rho}{\partial t},\frac{\partial u}{\partial t},\frac{\partial v}{\partial t}\right) \\ \frac{\partial}{\partial s}\left(\frac{v}{t}\right) &= \varphi_4\left(t,p,\rho,u,v,\frac{\partial p}{\partial t},\frac{\partial \rho}{\partial t},\frac{\partial u}{\partial t},\frac{\partial v}{\partial t}\right) \end{aligned}\right\} \tag{9}$$

For a given set of free-stream conditions and shock shape, the values of p,ρ,u, and v/t just behind the shock wave are calculated from the Rankine-Hugoniot relations, and the derivatives with respect to t are found by numerical differentiation. Then equations (9) are used to march in step-by-step toward the body. A flow chart for the computer program is shown in figure 1, and a list of subroutines is provided in table II. To illustrate the predictor-corrector integration technique, suppose the flow properties are known for the $(i - 1)$th and ith steps and are to be calculated for the $(i + 1)$th step (see sketch (b)). A second-order predictor and a modified Eulerian second-order corrector are used as follows, where p is a typical flow variable.

1. Differentiate numerically data for ith step to obtain $(\partial p/\partial t)_i$

2. Calculate from equations (9), $(\partial p/\partial s)_i$

3. Predict new value $\bar{p}_{i+1} = p_{i-1} + 2\,\Delta s(\partial p/\partial s)_i$

4. Differentiate numerically to obtain $(\partial \bar{p}/\partial t)_{i+1}$

5. Calculate from equations (9), $(\partial \bar{p}/\partial s)_{i+1}$

6. Correct value $p_{i+1} = p_i + 0.5\,\Delta s[(\partial p/\partial s)_i + (\partial \bar{p}/\partial s)_{i+1}]$

The stream function is calculated for each point, and the body is determined as the locus of points where the stream function vanishes. The step size is chosen so that the stagnation point is reached in approximately seven steps. It is usually necessary to iterate on the shock shape to obtain the desired body shape. However, this procedure is simplified by a one-parameter family of shock shapes that will produce reasonably accurate spheres and ellipsoids. Values of the shock-shape parameter for spheres are presented in reference 3 for perfect gases and for air in thermodynamic equilibrium. Solutions for other gases and nonspherical bodies including not-too-blunt ellipsoids can be obtained by appropriate changes of the shock-shape parameter. There are limitations on the application of the program, mainly because of inherent numerical difficulties, as discussed in reference 3. As a general rule, solutions are not possible for Mach numbers less than 3 and for body shapes that are either very blunt ($B_b > 4$) or not smooth in the nose region.

The output from the blunt-body program consists of the flow properties on the body and in the flow field at the coordinate intersections shown in sketch (b). In addition, the properties are interpolated along a line joining the shock and body in the supersonic region. These data can be used as input for the method of characteristics program to continue the calculations downstream over the afterbody.

METHOD OF SOLUTION FOR SUPERSONIC REGION

A computer program based on the method of characteristics is used to determine the flow field in the supersonic region. This program is comprised of a main program and 33 subroutines which are listed in table III. Most of these subroutines are short and straightforward and, therefore, they will not be explained in detail. (Table III describes the primary function of each.) However, the main program requires a few words of explanation. In addition, certain quadratic interpolation procedures as well as methods for calculating embedded shock waves will be discussed.

Calculation Procedure for Smooth Bodies

Along the characteristic or Mach lines, the partial differential equations ((1) through (3)) reduce to the following ordinary equations (see, e.g., ref. 11):

$$\frac{\cot \mu}{\rho V^2}\,dp \pm d\theta = -\frac{\epsilon \sin \theta}{M \sin(\theta \pm \mu)}\,\frac{dy}{y} \tag{10}$$

Equation (10) is solved in conjunction with the energy equation in integrated form

$$h + \frac{V^2}{2} = h_t = \text{constant} \tag{11}$$

the conservation of entropy on streamlines

$$S = S(n) \tag{12}$$

and the equation of state

$$h = h(p,S) \tag{13}$$

Briefly, the method consists of starting with flow properties along a non-characteristic line between the body and the shock wave, as determined from the solution for the subsonic-transonic region, and then integrating the equations downstream along the Mach lines. The stepwise procedure is illustrated by the typical characteristic mesh shown in sketch (c). Beginning with known data on the starting line the calculation proceeds to the body along a right-running characteristic, and then back to the next starting point (or shock point). A simple flow chart is shown in figure 2 which illustrates this part of the program logic. In sketch sketch (c), the previously calculated (or input) data points are identified by small circles, and the point currently being calculated is identified by the shaded symbol. Only the numbered points are available in computer memory at this time, the remaining circled points having been written out previously. The stored data points are contained in a two-dimensional array, P(J,K), in which the index J identifies the various flow variables and the index K identifies the location of the point. In terms of program terminology, the number of field points involved in the calculation loop is given by M2 + 1, where M2 is an integer defined in the main program. The field point currently being calculated is identified as P(J,K9), where K9 is also an integer defined in the main program. Thus as the calculation proceeds along a right-running characteristic, the integer K9 takes on successive values between K9 = M2 + 1 on the shock (or input line) to K9 = 1 on the body.

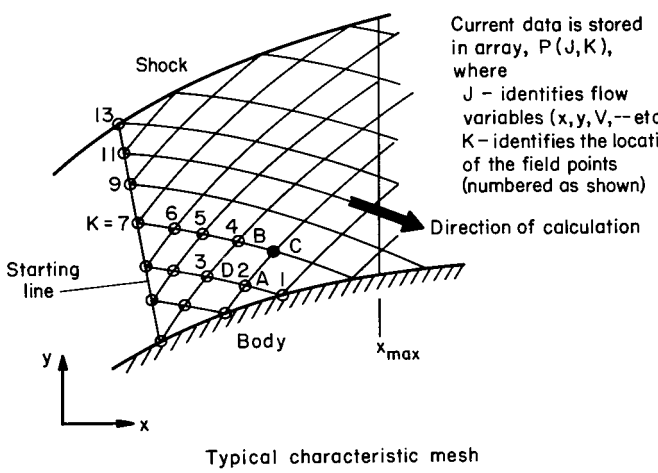

Typical characteristic mesh

Sketch (c)

For the calculation of a typical mesh point (C in sketch (c)), three adjacent points are usually used. These points are labeled A,D,B in sketch (c), and correspond, in the example shown, to the points K = 2,3,4 in

the P array. The calculation of data at the new point is effected with the use of equations (10) through (13) and a standard predictor-corrector procedure which averages the coefficients of the differentials. The procedure is started with a crude predictor (i.e., that conditions at C equal those at B) and is followed, therefore, by at least two correctors. This is in contrast to the method used for the blunt-body solution which makes use of only one corrector, but which uses a second-order predictor.

In calculating rotational supersonic flow by the method of characteristics, it is convenient to introduce entropy as a flow property since it remains constant on streamlines. In the past it has sometimes been assumed that the entropy varies linearly between streamlines (see ref. 16, p. 636). To illustrate this procedure, consider three points in the flow field (see sketch (c)) A and B, where the flow properties are known, and C, where the flow properties are to be determined. The entropy at C can be calculated using the flow properties at A and B and with the assumption that the entropy varies linearly along the normal to the streamlines between A and B. This assumption is valid provided that the change in entropy gradient between A and B is small. However, serious errors may occur in the flow-field calculations if this condition is not realized (see, e.g., ref. 17). Decreasing the mesh size by increasing the number of mesh points is not a satisfactory remedy because the computing time increases as the square of the number of input points, and the storage capacity of computing machines is also limited. In reference 17, an iterative scheme was used wherein a check on the integrated mass flow was made point by point throughout the field. The method adopted in the present program is simpler in that no additional iterations are needed. Quadratic rather than linear interpolation for the entropy is used, and errors are therefore reduced to the order of the cube of the mesh size. This is accomplished by using the flow properties at point D, which lies on Mach lines upstream from A and B. This additional point allows the use of a quadratic calculation for entropy between A and B. Some improvement in the flow-field solution can be expected, especially in regions where large changes in entropy gradient occur.

A feature of the present computer program, which proved useful for examining entropy gradients, is the ability to interpolate for field data on radial (body- or axis-normal) lines. This operation is noted in the flow chart (fig. 2). These interpolated data at several x stations are printed out at the end of the normal output and, if desired, the data from the last x station can be stored on magnetic tape. This tape can later be used to provide starting conditions to extend the calculation downstream.

Calculation Procedure for Bodies With Corners

The method of characteristics described in the previous section is not applicable in regions where the body slope is discontinuous, or where embedded shocks occur. For these cases, characteristics theory may be applied on both sides of the discontinuity with matching conditions obtained for the Rankine-Hugoniot shock relations, or Prandtl-Meyer equations in the case of an expansion corner. Methods for calculating flows of this type may be found, for

example, in reference 16. This section describes some of the details of this calculation as incorporated into the present program.

While any number of discontinuities are allowable in theory, practical considerations have resulted in a limitation, for the present program, of any two of the discontinuities indicated in sketch (a). These are: (a) an expansion corner, (b) a compression corner, and (c) an embedded shock arising, for example, from a coalescence of Mach waves from a concave wall. Procedures used in calculating these three types of discontinuities are discussed next. Descriptions of the compression corner and coalesced shock explain only the starting conditions used for the shock calculation, and are followed by an explanation of a general embedded shock point. The calculation for an embedded shock proceeds to its intersection with the bow shock. Then, since interactions between shocks are not considered, the calculation terminates along a right-running characteristic through this point.

Expansion corner.- The expansion corner is illustrated in sketch (d). Upon reaching the body in region II for the first time, point C is calculated on the extension of the body shape specified for region I. This provides an analytic continuation of the flow ahead of the corner and, with stored data at points A and B, enables one to use a quadratic interpolation for conditions at point D just ahead of the corner. Now, given conditions at D and the expansion angle δ, the Prandtl-Meyer equations can be used to calculate conditions on the body just behind the corner. In addition, conditions for several intermediate angles are computed and all are stored with coordinate values corresponding to point D. The problem is now reduced to one which can be handled by the main characteristics program. With known conditions at points D and E, point F can be computed, followed by similar calculations for points G,H, etc., until the entire expansion fan is determined as shown in the inset. A greater number of mesh points are introduced at such a corner for large expansion angles, so as to provide a reasonably uniform mesh.

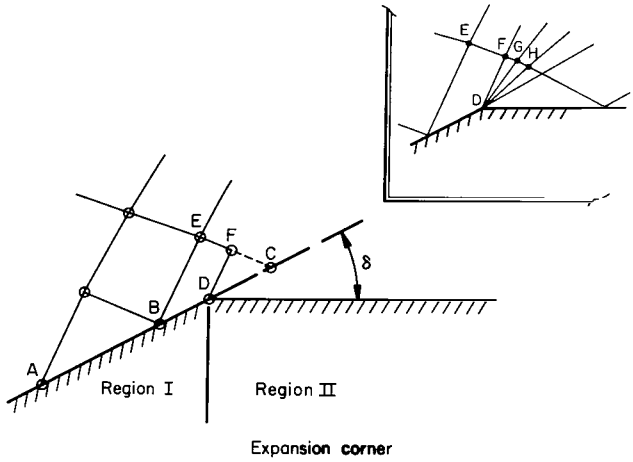

Sketch (d)

Compression corner.- The compression corner is shown in sketch (e). The procedure for calculating conditions at point D is identical with that described for the expansion corner. In this case, the oblique shock relations are used to calculate the flow variables on the body just behind the corner in terms of upstream conditions at point D and the known deflection angle, δ. The necessary shock solution is not explicit, however, and an iterative procedure has been programmed to give the jump conditions. The segment of the shock D-F is assumed straight and at an angle corresponding to the oblique shock at point D. Data at point F are then found by a quadratic

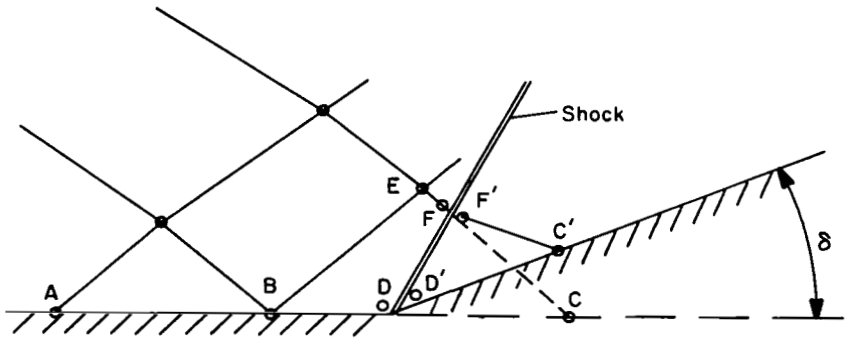

Compression corner

Sketch (e)

interpolation along the right-running characteristic through E, and the jump conditions at point F are computed from the shock relations. The data at D' and F' can now be used to determine the body point C'. Knowledge of the shock wave at point F must be stored in the main computer program so that the general shock-point subroutine can be called when the calculation along the next right-running characteristic reaches this point.

Coalesced shock.- In sketch (f) the formation of a coalesced shock in the flow field is depicted at point E where two Mach lines of the same family have intersected. A shock wave is started at point E and at an angle equal to the average slope of the Mach lines F-E and G-E. The jump conditions at A-A' are then computed and stored in the P array. Now the points numbered (K9 - 3),(K9 - 4), and so on, are computed with the use of known data on the characteristic through point G. This procedure gives the starting conditions for the coalesced shock, and the problem is now reduced to the general case which is explained next.

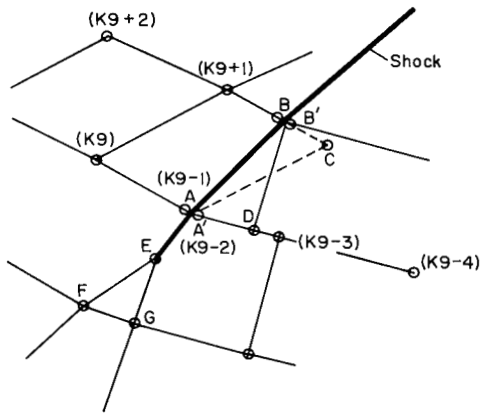

General shock point

Sketch (f)

General shock point.- This subroutine solves, in an iterative procedure, for the shock angle at point B in sketch (f), which satisfies the flow conditions behind the shock. The procedure is as follows. When the shock is reached, point C is first calculated in the usual way with data at (K9 - 1), K9, and (K9 + 1). After an initial guess, the average shock angle at A and B is used to locate point B, and data there are obtained by quadratic interpolation through points C, (K9 + 1), and (K9 + 2). Data at B' are obtained from the shock relations, and the intersection D of Mach lines through A'

and B' is determined. Data at point D are obtained by interpolating through points A',(K9 - 3), and (K9 - 4). Equation (10) is then used to determine conditions at B' in terms of data at D, that is, on the line D-B'

$$\frac{\cot \mu}{\rho V^2} dp + d\theta = - \frac{\epsilon \sin \theta}{M \sin(\theta + \mu)} \frac{dy}{y}$$

The value of pressure at B' obtained from this equation is then compared with that obtained from the shock conditions and the iteration is continued until the two values agree. The calculation on the downstream side of the shock can then proceed in the usual way.

RESULTS AND DISCUSSION

Effect of Entropy Calculation on Solutions for a Perfect Gas

The flow field around a blunted cone is quite sensitive to the entropy calculation because of the growth of the body shape. Since the total amount of high entropy fluid remains constant, the thickness of the entropy layer must diminish as the body radius grows. Consequently, the entropy gradients normal to streamlines must increase.

The flow field over a spherically blunted cone was calculated by the present method for $\gamma = 1.4$ and $M_\infty = 10$. Both the shock-wave shape and surface-pressure distribution were unaffected by the entropy calculation. However, the total pressure profiles in the shock layer are significantly different as shown in figure 3(a). (The ordinate is the distance from the surface normalized by the total distance to the shock.) The differences are associated with the overexpansion of the shock wave which occurs near $x/R = 10$. The entropy rise across the shock wave is a minimum there, and, hence, the total pressure in the shock layer has the maximum value of $2.1 \times 10^4 \times p_\infty$ on the streamline passing through this point. At every downstream station, the total pressure on this streamline must have the same value. The linear entropy interpolation smooths the total pressure distribution and erroneously reduces this maximum value. Past $x/R = 40$, the entropy layer becomes so thin that even quadratic interpolation is not accurate near the body. This deficiency is usually unimportant from a practical standpoint because the inviscid entropy layer would have been absorbed within the boundary layer.

The static pressure profiles are not affected by the entropy calculation as shown in figure 3(b). However, the entropy calculation has a significant effect on the density and velocity profiles shown in figures 3(c) and 3(d). The result is that the mass-flow balance between the shock layer and the free stream deteriorates with distance as shown in figure 4. At $x/R = 25$, the error in the mass-flow balance is 9 percent with linear interpolation and negligible with quadratic interpolation.

Similar comparisons have been made for a hemisphere cylinder for which the entropy gradients are not as large. Linear interpolation for the entropy yielded satisfactory results for the shock-wave shape, surface-pressure distribution, shock-layer profiles, and mass-flow balance. These results corroborate the findings of reference 5 where linear interpolation for the entropy was used, and checks of the mass-flow balance showed satisfactory agreement. These examples show that for most bodies linear interpolation for the entropy is adequate for obtaining shock-wave shape and static-pressure distribution, but it may cause serious errors in the other flow-field properties in regions with large entropy gradients. Since quadratic interpolation does not require an appreciable increase in the computing time, it is used exclusively in the present method.

Comparison of Results From Present Method With Chushkin and Shulishnina

It is of interest to compare results from the present method with other calculations. Flow-field calculations by the method of characteristics for blunted cones by Chushkin and Shulishnina (ref. 6) were recently brought to our attention. These calculations differ from the present method in that the subsonic-transonic solution was that obtained by Belotserkovskii (ref. 4) using the method of integral relations. In addition, some differences are to be expected in the computational procedure for the method of characteristics. Solutions were obtained for spherically blunted cones with half angles ranging from 0° to 40° and for $\gamma = 1.4$ and $M_\infty = 4$, 6, and 10. The surface-pressure distributions in the nose region from reference 6 and the present method are in good agreement as shown in figure 5. Although not shown in the figure, this good agreement extends downstream until the sharp-cone values are reached.

Comparisons of pressure distributions over cylinders with ellipsoidal noses are shown in figure 6 for $\gamma = 1.4$ and $M_\infty = 6$. For the slender or prolate ellipsoid, the calculations proceeded smoothly, and the results from the present method show good agreement with the results of reference 6. For the blunt or oblate ellipsoid, the blunt-body solution used in the present method is in error in the transonic region. However, the method of characteristics solution quickly corrects this error, at least, as far as the surface pressure is concerned.

Comparison With Experiment for a Body With Corners

As an illustration of the embedded shock and expansion fan calculations, the flow over a blunt cone-cylinder-flare body was calculated for perfect air at a Mach number of 4.10. The results of the shock shapes obtained from this calculation are shown in figure 7, and the surface pressures are shown in figure 8. Also shown in these figures are experimental results from reference 18. Of particular interest in figure 7 is the good agreement between experiment and theory for the embedded shock on the flare. Good agreement is also found for the experimental and calculated pressure distributions in figure 8. Note that the calculation predicts an increasing pressure with distance along the flare. This pressure variation is caused by the increase of

upstream dynamic pressure with distance from the corner, that is, the effect of the nonuniform upstream conditions created by the strong bow shock (cf. ref. 9).

Example of Solution for Gas Mixtures in Thermodynamic Equilibrium

Flow-field solutions for gases in thermodynamic equilibrium present no inherent difficulty aside from an increase in computing time required to calculate the thermodynamic properties. However, the limited accuracy of the real gas properties obtained from the curve fits coupled with the different calculation methods used in the blunt body and method of characteristics programs may result in an incompatibility along the input line. For example, in the blunt-body program the enthalpy is determined with pressure and density as inputs, whereas in the method of characteristics program the enthalpy is determined with pressure and entropy as inputs. In regions where the curve fits are poor, particularly near the limits of the tables, the two values for enthalpy may be substantially different and may cause difficulties.

As examples of flow-field calculations for real gases, the pressure distribution on the blunt cone-cylinder-flare body studied in the preceding example is shown in figure 9 for air and for a mixture of nitrogen and carbon dioxide. No unusual effects are noted compared with the earlier perfect gas results.

CONCLUDING REMARKS

The Ames computer programs for calculating the complete subsonic-supersonic flow field around blunt-nosed bodies at zero angle of attack were described. The more complex portions of the programs were explained in detail, and flow charts for the main programs were presented. The flow charts should be helpful in diagnosing difficulties or making minor modifications for specific applications.

A number of example calculations were presented to illustrate the applicability and accuracy of the programs. It was shown that the use of a quadratic rather than the usual linear interpolation for entropy improved the accuracy of the method of characteristics program. The improvement showed up especially in the total pressure near the surface of blunt cones, where large entropy gradients develop, and in the integrated mass flow across the shock layer for such bodies. Surface-pressure distributions on blunted cones are in agreement with published numerical results obtained by somewhat different methods. Surface pressures and shock shapes, including the embedded shock, for a blunted cone-cylinder-flare, show good agreement with experiment.

Finally, to illustrate applicability to flows of real gases in thermodynamic equilibrium, surface pressures on a flared body were presented for flight in air and in a CO_2-N_2 mixture.

Ames Research Center
National Aeronautics and Space Administration
Moffett Field, Calif., June 8, 1965

REFERENCES

1. Van Dyke, Milton D.: The Supersonic Blunt-Body Problem - Review and Extension. J. Aerospace Sci., vol. 25, no. 8, Aug. 1958, pp. 485-496.

2. Batchelder, R. A.: An Inverse Method for Inviscid Ideal Gas Flow Fields Behind Analytic Shock Shapes. SM-42588, Missile and Space Systems Div., Douglas Aircraft Co., Inc., July 1963.

3. Lomax, Harvard; and Inouye, Mamoru: Numerical Analysis of Flow Properties About Blunt Bodies Moving at Supersonic Speeds in an Equilibrium Gas. NASA TR R-204, 1964.

4. Belotserkovskii, O. M.: The Calculation of Flow Over Axisymmetric Bodies With a Detached Shock Wave. Computation Center, Acad. Sci., Moscow, USSR, 1961. Translated and edited by J. F. Springfield, RAD-TM-62-64, AVCO Corp., 1962.

5. Inouye, Mamoru; and Lomax, Harvard: Comparison of Experimental and Numerical Results for the Flow of a Perfect Gas About Blunt-Nosed Bodies. NASA TN D-1426, 1962.

6. Chushkin, P. I.; and Shulishnina, N. P.: Tables of Supersonic Flow About Blunted Cones. Computation Center Monograph, Acad. Sci., Moscow, USSR, 1961. Translated and edited by J. F. Springfield, RAD-TM-62-63, AVCO Corp., 1962.

7. Eastman, D. W.; and Radke, L. P.: Effect of Nose Bluntness on the Flow Around a Typical Ballistic Shape. AIAA J., vol. 1, no. 10, Oct. 1963, pp. 2401-2402.

8. Palermo, D. A.: Equations for the Hypersonic Flow Field of the Polaris Re-Entry Body. LMSD-480954, Lockheed Missiles and Space Div., Lockheed Aircraft Corp., Oct. 1960.

9. Seiff, A.: Secondary Flow Fields Embedded in Hypersonic Shock Layers. NASA TN D-1304, 1962.

10. Jorgensen, Leland H.; and Graham, Lawrence A.: Predicted and Measured Aerodynamic Characteristics for Two Types of Atmosphere-Entry Vehicles. NASA TM X-1103, 1965.

11. Hayes, Wallace D.; and Probstein, Ronald F.: Hypersonic Flow Theory. Academic Press, New York, 1959.

12. Marrone, Paul V.: Inviscid, Nonequilibrium Flow Behind Bow and Normal Shock Waves, Part I. General Analysis and Numerical Examples. CAL Rep. QM-1626A-12(I), May 1963.

13. Bailey, Harry E.: Equilibrium Thermodynamic Properties of Carbon Dioxide. NASA SP-3014, 1965.

14. Walsh, J. L.; Ahlberg, J. H.; and Nilson, E. N.: Best Approximation Properties of the Spline Fit. J. Math. Mech., vol. 11, no. 2, March 1962, pp. 225-234.

15. Hilsenrath, Joseph, et al.: Tables of Thermal Properties of Gases... Cir. 564, U.S. National Bureau of Standards, Nov. 1, 1955.

16. Ferri, Antonio: The Method of Characteristics, Section G. Supersonic Flows With Shock Waves, Section H. General Theory of High Speed Aerodynamics, William R. Sears, ed., Princeton University Press, Princeton, New Jersey, 1954, pp. 583-747.

17. Powers, S. A.; and O'Neill, J. B.: Determination of Hypersonic Flow Fields by the Method of Characteristics. AIAA J., vol. 1, no. 7, July 1963, pp. 1693-1694.

18. Inouye, Mamoru; and Sisk, John B.: Wind-Tunnel Measurements at Mach Numbers From 3 to 5 of Pressure and Turbulent Heat Transfer on a Blunt Cone-Cylinder With Flared Afterbody. NASA TM X-654, 1962.

TABLE I.- GAS MIXTURES ON AMES REAL-GAS TAPE

Composition by volume in percent			File number
Air: 78.2 N_2, 21.8 O_2			2
Nitrogen	Carbon dioxide	Argon	
100			1
95.1	4.9		11
90	10		4
89.2	10.8		12
80	20		7
70	30		8
60	40		9
51.2	48.8		13
50	50		10
40	10	50	6
	100		3
		100	5

TABLE II.- LIST OF SUBROUTINES

BLUNT-BODY PROGRAM

	Subroutine name and ID no. (if any)	Primary calling routine	Subroutine function
1	EXEC1(TH0701)	MAIN	Reads input cards
2	EXEC2(TH0702)	MAIN	Reads shock-shape parameters and calculates shock shape and slope
3	OUT(TH0704)	MAIN DERIVT	Outputs free-stream conditions and field data after each step
4	SHOCK(TH0705)	MAIN	Calculates flow properties behind shock wave
5	DERIVS(TH0706)	MAIN STEP	Calculates derivatives in s direction
6	FIELDS(TH0707)	BODYS	Calculates coefficients for line on which output data is desired
7	STEP(TH0708)	MAIN	Predicts and corrects the flow variables for the following step
8	BODYS(TH0709)	STEP	Calculates body location and flow properties
9	POLYN(TH0710)	EXEC2	Evaluates polynomial and first two derivatives for given value of argument
10	FIELDP(TH0711)	BODYS	Interpolates field data to find properties on output line
11	BODYS1(TH0712)	BODYS	Smooths body coordinates
12	FHIPSI(TH0713)	STEP	Calculates stream function
13	TERP3(TH0714)	SHOCK FIELDS FIELDP SONIC	Interpolates using 3-point Lagrange method
14	SONIC(TH0715)	BODYS	Locates sonic line
15	OUT7(TH0716)	MAIN	Outputs data for body and along output line
16	DERIVT(TH0717)	MAIN STEP	Differentiates numerically to obtain derivatives in t direction
17	FIELDX(TH0718)	BODYS	Stores starting data for the method of characteristics on tape
18	POLY3(TH0720)	MAIN FIELDP	Evaluates coefficients for second degree polynomial passing through three given points
19	LES2N(TH0723)	BODYS	Evaluates coefficients for least-squares fit straight line
20	SMOOTH(TH0724)	BODYS1 DERIVT	Smooths data by filtering out high frequency oscillations
21	DERIV1(TH0725)	BODYS1 DERIVT	Calculates derivative using 5 points
22	DIFFOR(TH0733)	OUT	Calculates fourth differences

TABLE II.- LIST OF SUBROUTINES

BLUNT-BODY PROGRAM - Concluded

	Subroutine name and ID no. (if any)	Primary calling routine	Subroutine function
23	ENQ55R(TH0737)	BODYS1	Obtains running integral of equally-spaced data
24	RGAS	EXEC1, SHOCK, DERIVS, BODYS, FIELDP, OUT7	Calculates thermodynamic properties
25	SERCH	RGAS	Searches for coefficients for real-gas properties
26	LOCATE	FIELDX, RGAS	Locates tape at specified file position

TABLE III.- LIST OF SUBROUTINES

METHOD OF CHARACTERISTICS PROGRAM

	Subroutine name and ID no. (if any)	Primary calling routine	Subroutine function
1	EXEC	MAIN	Reads input cards, reads input tapes, initializes variables
2	EXEC2(TH2485)	MAIN	Reads additional input data
3	TOP	MAIN	Locates new bow shock point and calculates the new shock angle
4	MID	MAIN	Locates new mesh points and iterates for solution of equation (10)
5	BOT(TH2423)	MAIN	Locates new body point and iterates for body data
6	ESHOCK	MAIN	Keeps track of embedded shocks and adjusts storage locations in P array; interpolates for conditions on the body upstream of a corner
7	GSHOCK	ESHOCK	Locates general embedded shock point and calculates new shock angle
8	CSHOCK	ESHOCK	Calculates shock angle at a corner, and at the first mesh point away from the corner
9	EXPAN	ESHOCK	Calculates additional points for an expansion corner, and adjusts storage locations in P array
10	SHOCK	TOP, GSHOCK, CSHOCK	Calculates the shock jump conditions given the shock angle and upstream conditions
11	PM2	EXPAN	Calculates Prandtl-Meyer flow given the expansion angle and upstream conditions
12	RGAS		Calculates gas properties; reads RGAS tape
13	ROOTB(TH2426)	BOT	Locates intersection of right-running characteristic with the body
14	CON(TH2411)	MID	Calculates averages of the coefficients of equation (10)
15	DATA(TH2425)	EXEC	Reads starting flow-field data if specified on cards
16	TPRES(TH2429)		Calculates total pressure
17	ISENC	TPRES, PM2	Calculates one-dimensional isentropic flow between given velocities
18	ESPAC1(TH2409)	EXEC	Prepares data for equal spacing
19	ESPACE(TH2412)	ESPAC1	Equally spaces data with respect to a given variable
20	NTERP		Interpolating routine
21	TERP3(TH2405)		Interpolating routine

TABLE III.- LIST OF SUBROUTINES

METHOD OF CHARACTERISTICS PROGRAM - Concluded

	Subroutine name and ID no. (if any)	Primary calling routine	Subroutine function
22	TERP4(TH2406)	}	
23	POLY3(TH2408)	}	Interpolating routines
24	HERM	}	
25	ENQ55R(TH0737)		Integration routine
26	SHOCKP(TH2487)	MAIN	Interpolates for data at prescribed points along the bow shock
27	BODYP(TH2488)	MAIN	Interpolates for data at prescribed points along the body
28	SEARCH(TH2489)	MAIN	Interpolates for data along a characteristic line
29	SERCH1(TH2416)	BODYP	Calculates equations of body normal probe lines
30	PRINTF(TH2486)	MAIN	Stores data along body or axis normals; stores last probe on tape
31	SERCH	RGAS	Scans RGAS table for pertinent data
32	PLOTS	MAIN	Dummy subroutine - can be used to write a plot tape using data in P array
33	LOCATE	EXEC, PRINTF	Locates specified file positions on data storage tape

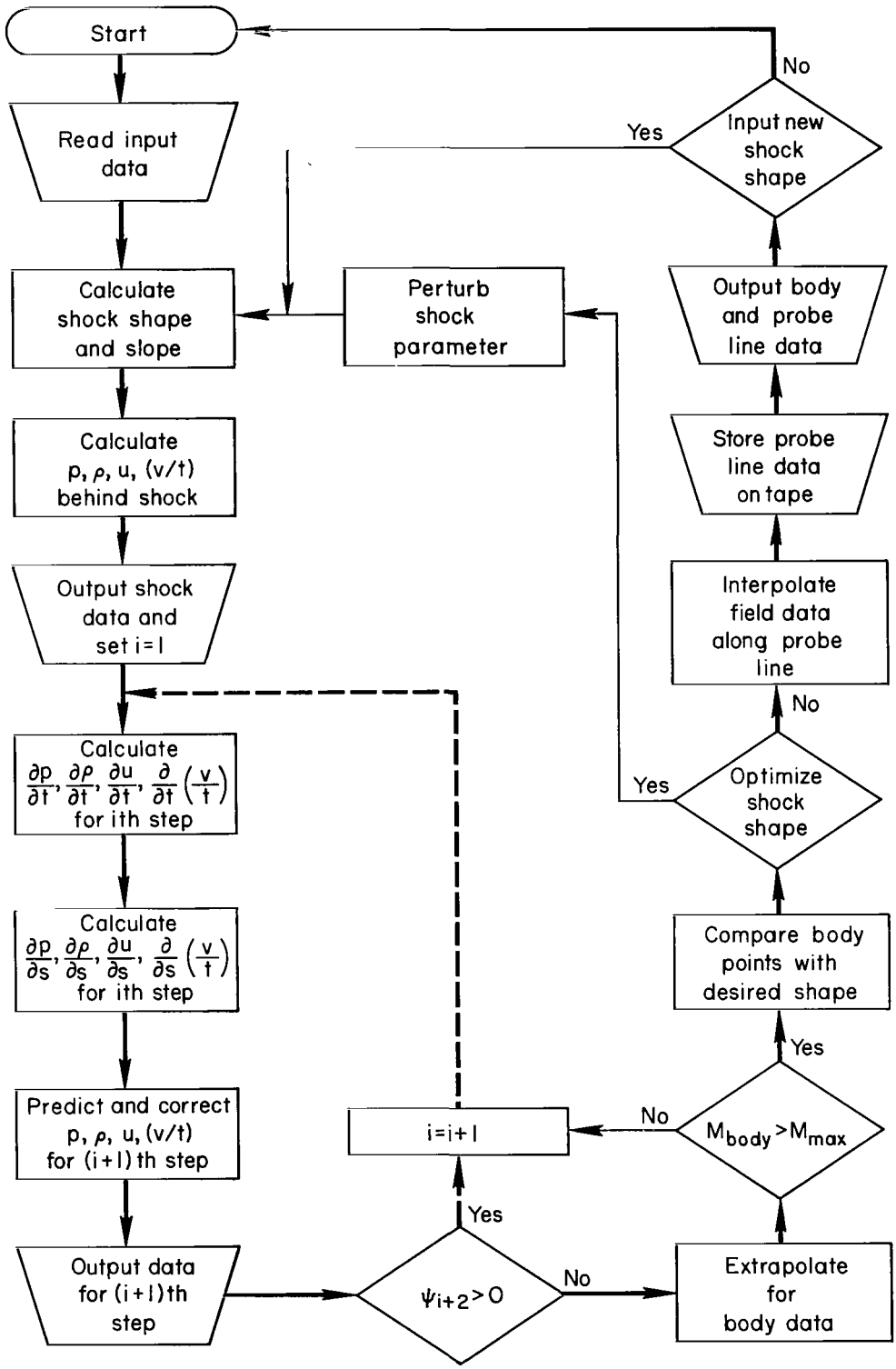

Figure 1.- Flow chart for blunt-body program.

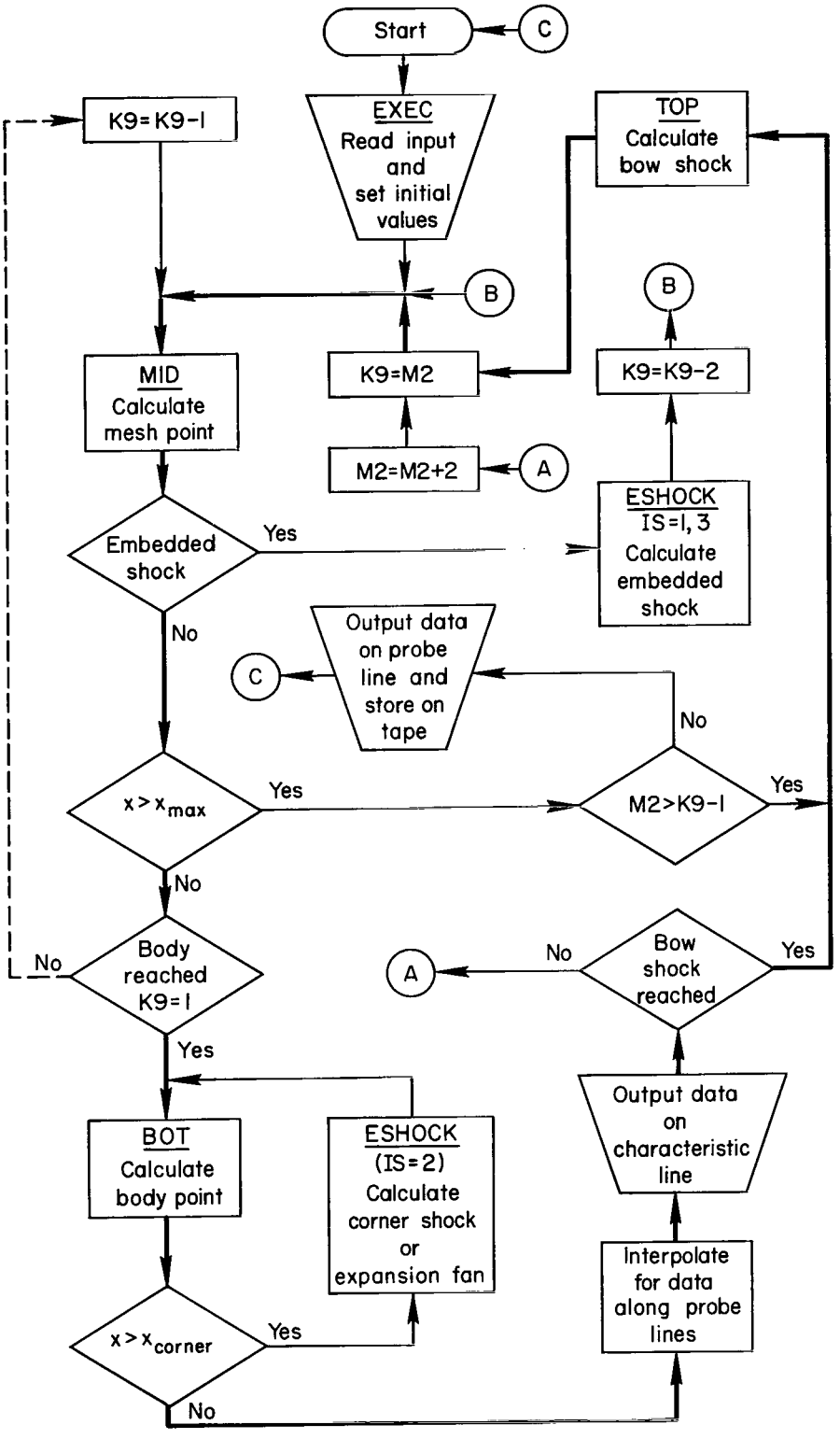

Figure 2.- Flow chart for characteristics program.

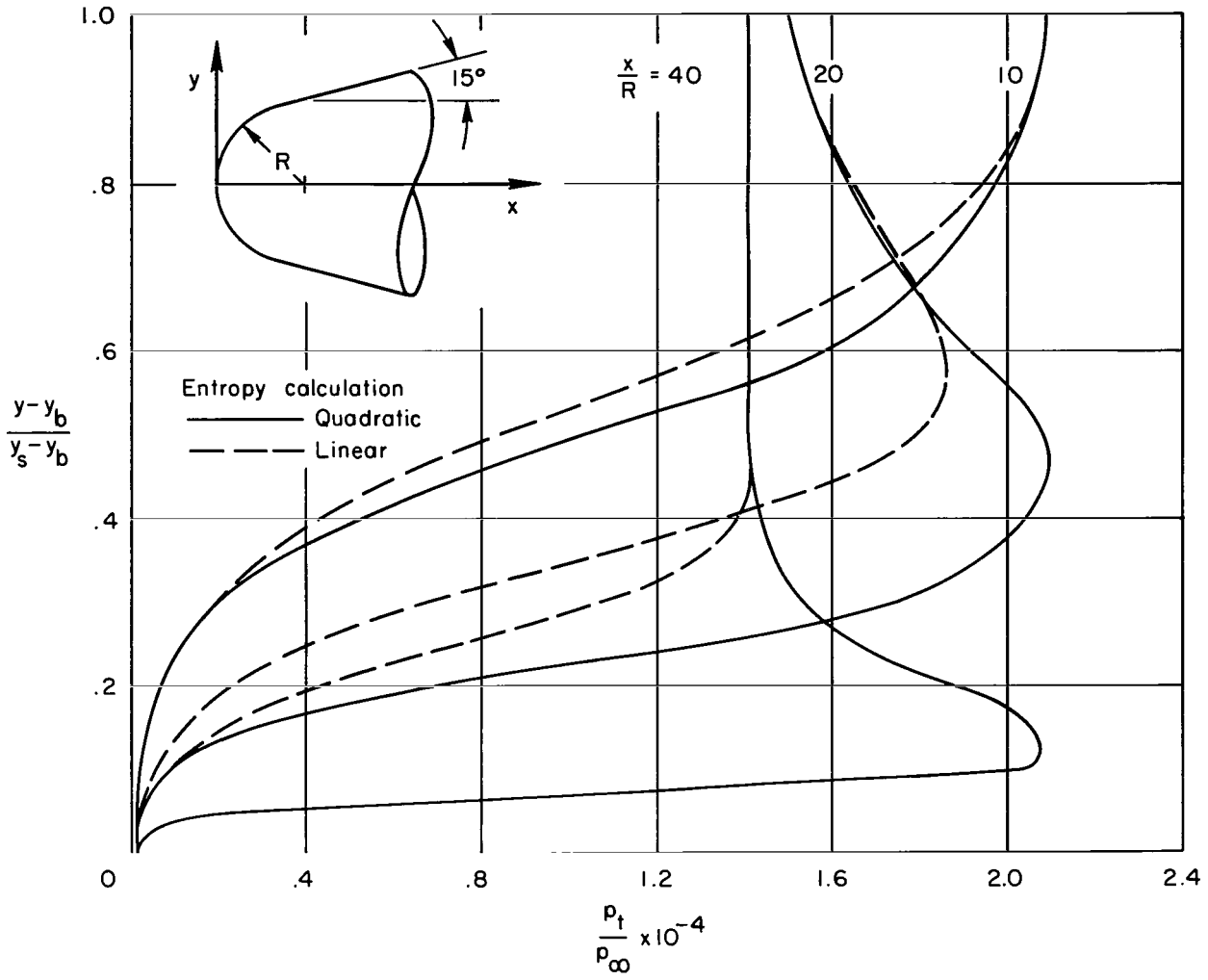

(a) Total pressure.

Figure 3.- Shock-layer distributions normal to axis for blunted cone; $\theta_c = 15^\circ$, $\gamma = 1.4$, $M_\infty = 10$.

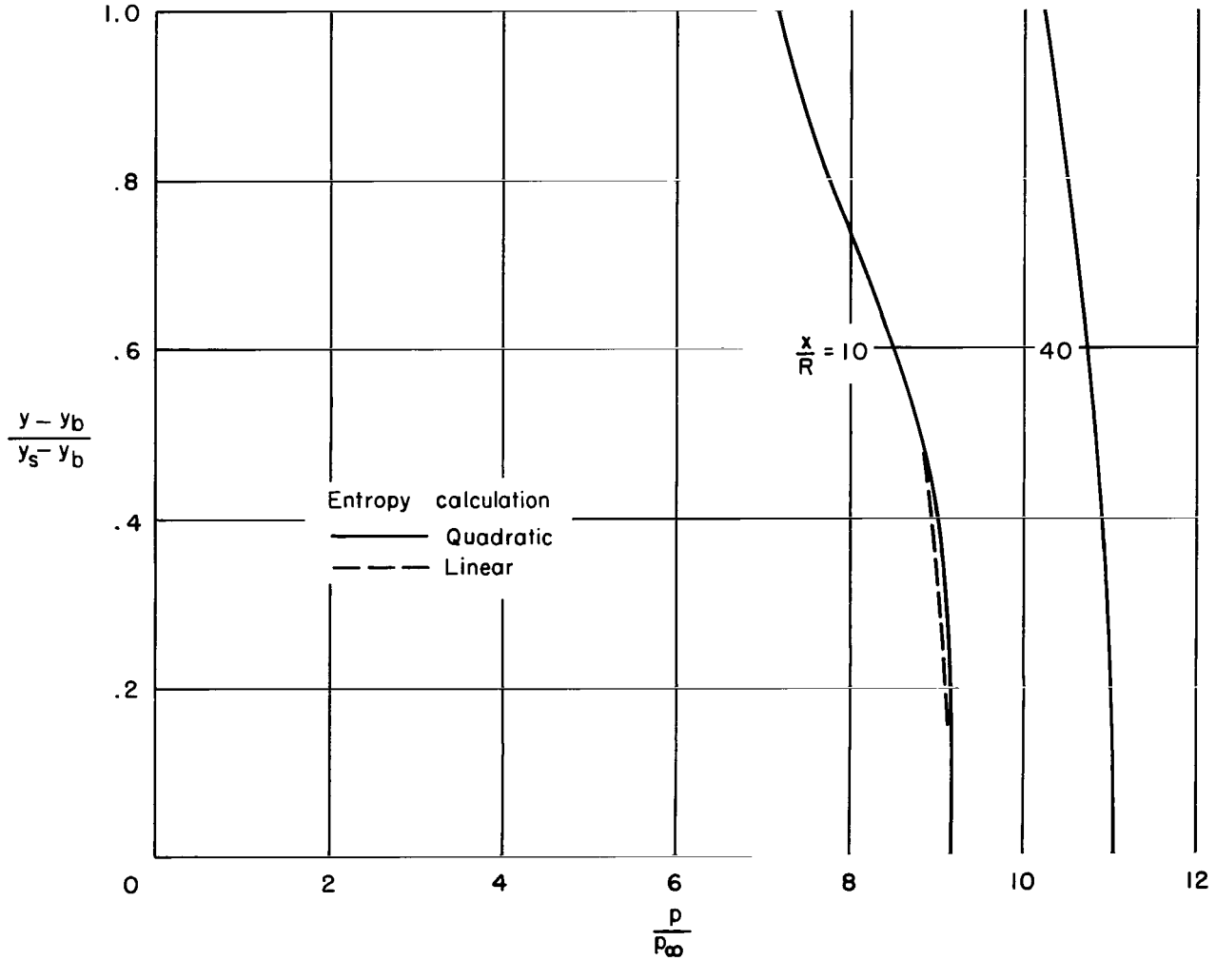

(b) Static pressure.

Figure 3.- Continued.

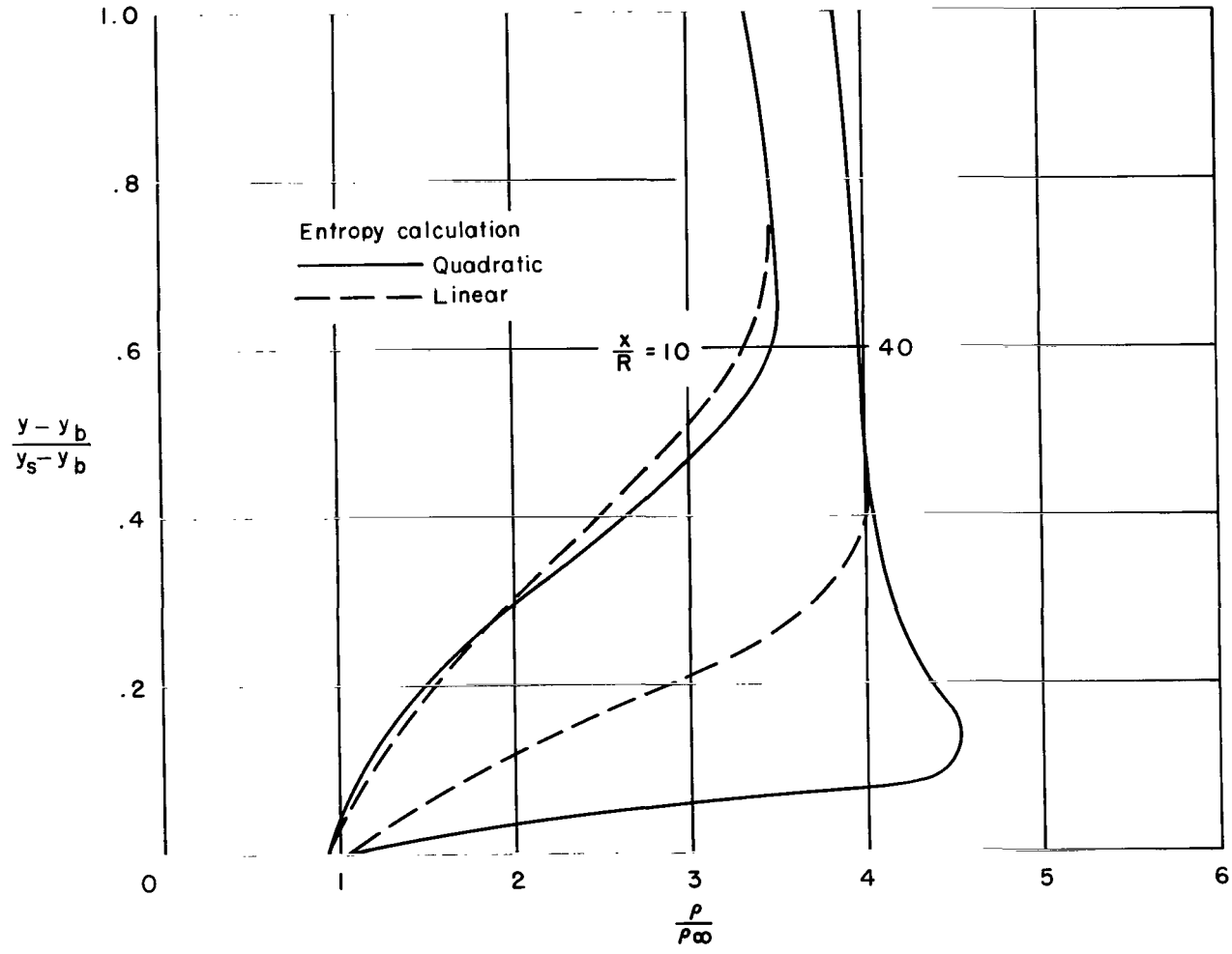

(c) Density.

Figure 3.- Continued.

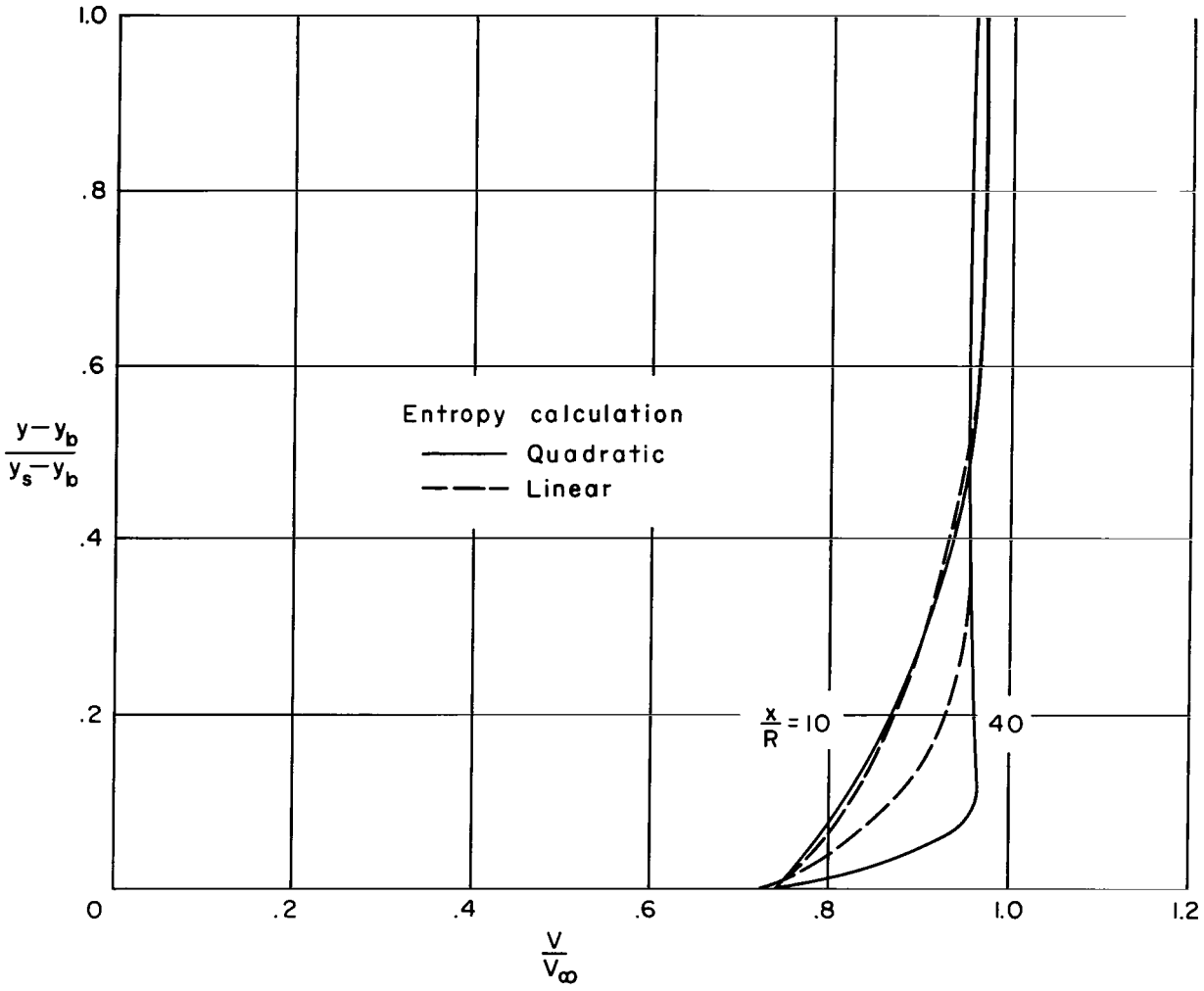

(d) Velocity.

Figure 3.- Concluded.

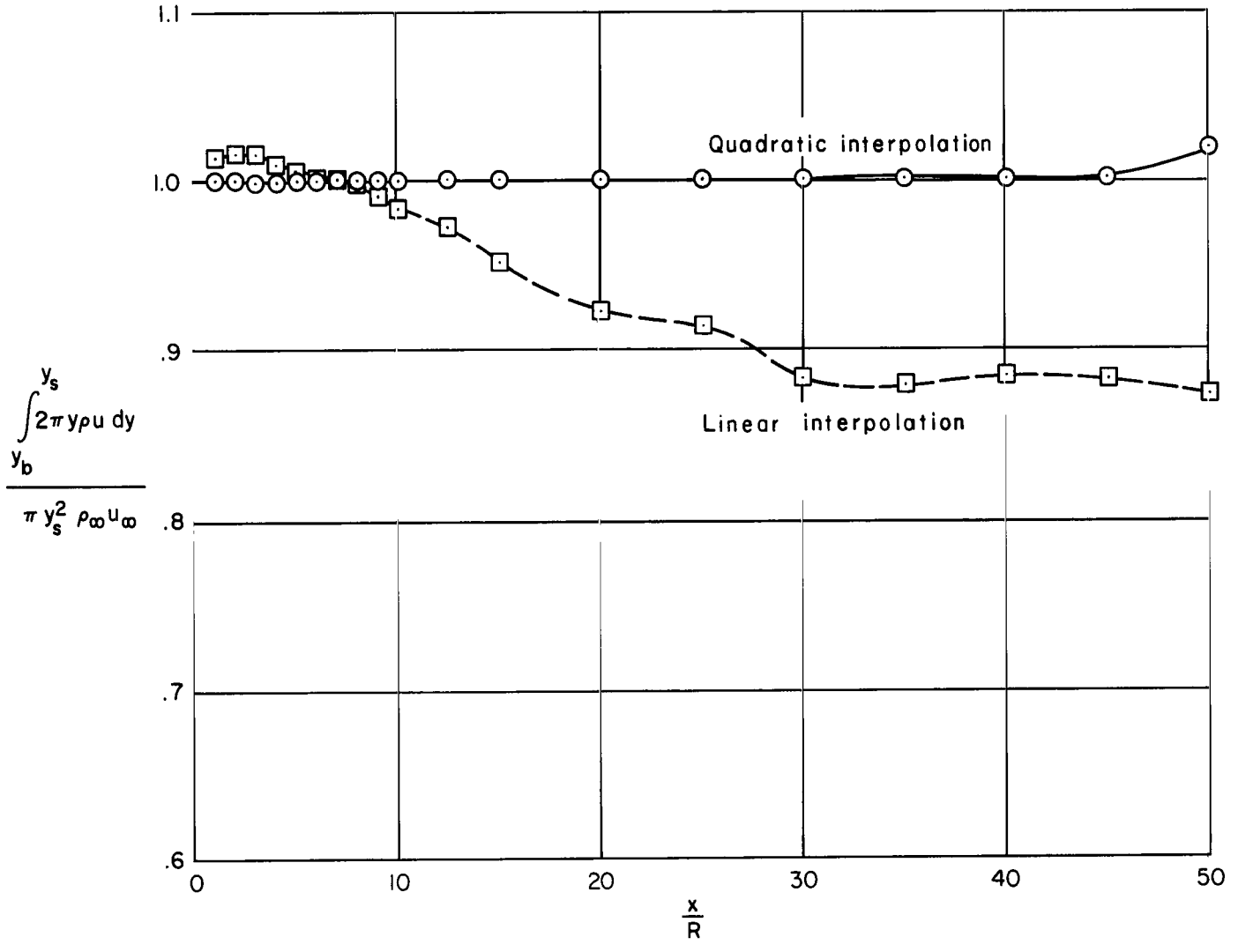

Figure 4.- Effect of entropy calculation on mass flow balance for blunted cone; $\theta_c = 15^\circ$, $\gamma = 1.4$, $M_\infty = 10$.

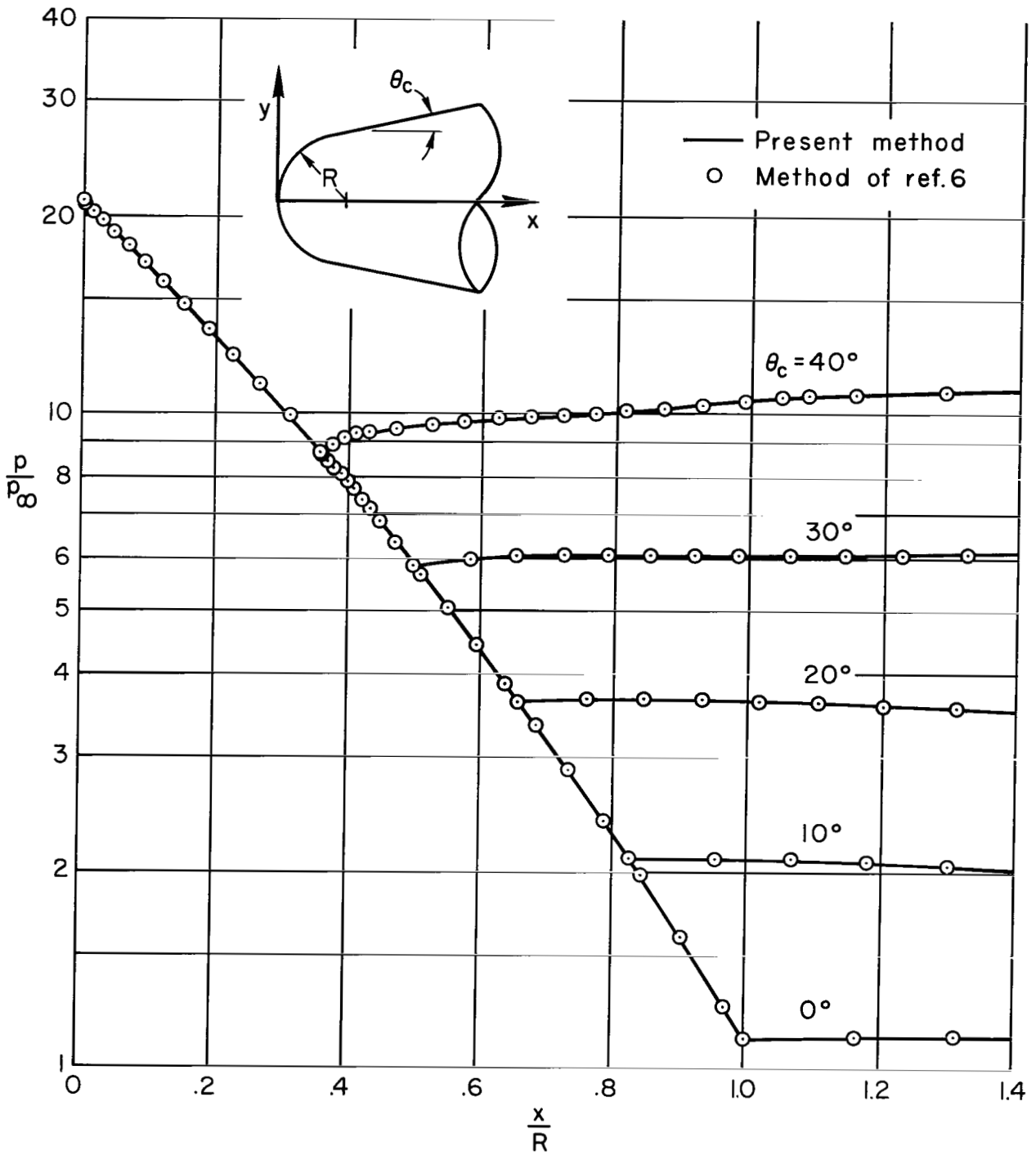

(a) $M_\infty = 4$

Figure 5.- Surface-pressure distribution on blunted cone, $\gamma = 1.4$.

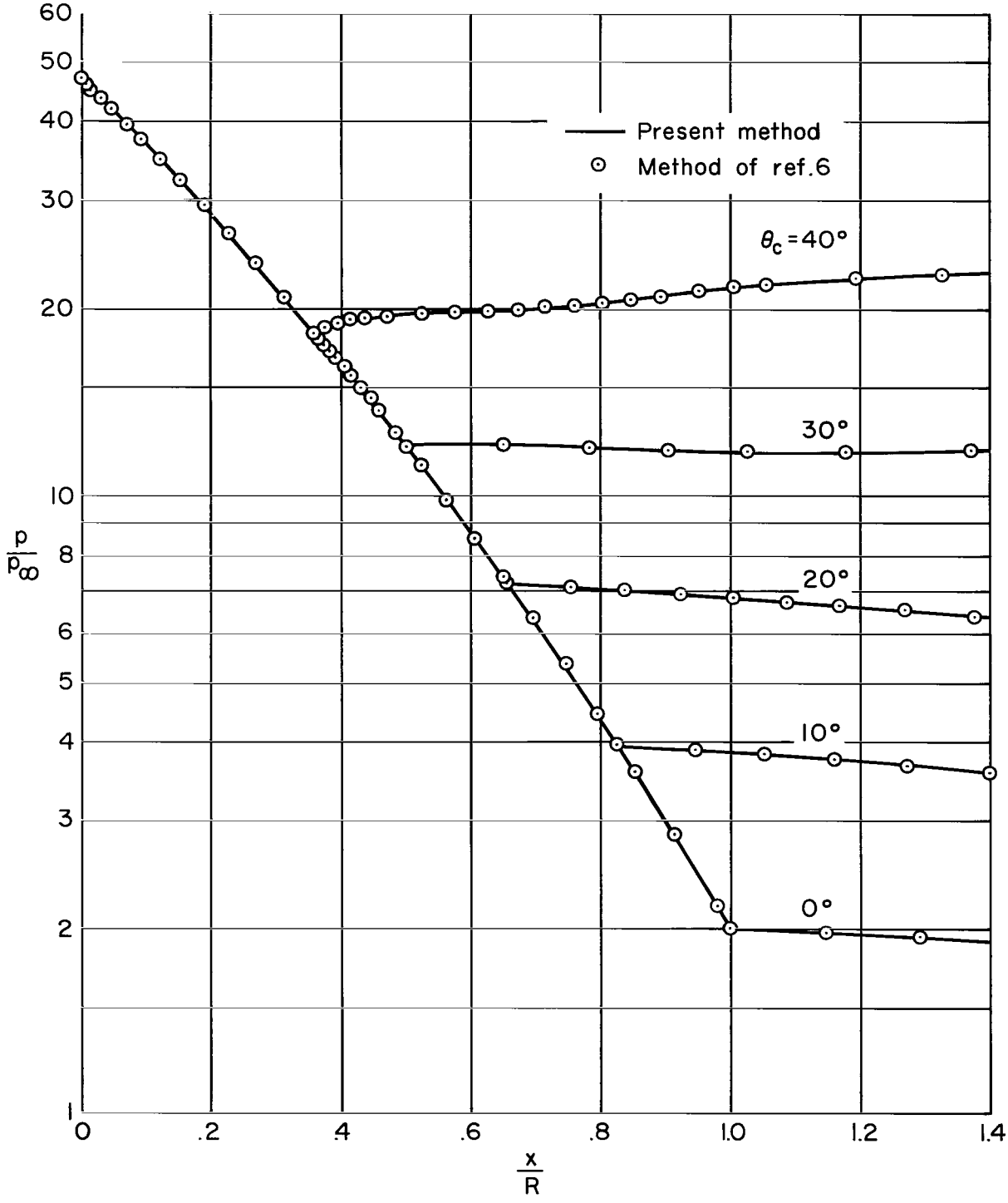

(b) $M_\infty = 6$

Figure 5.- Continued.

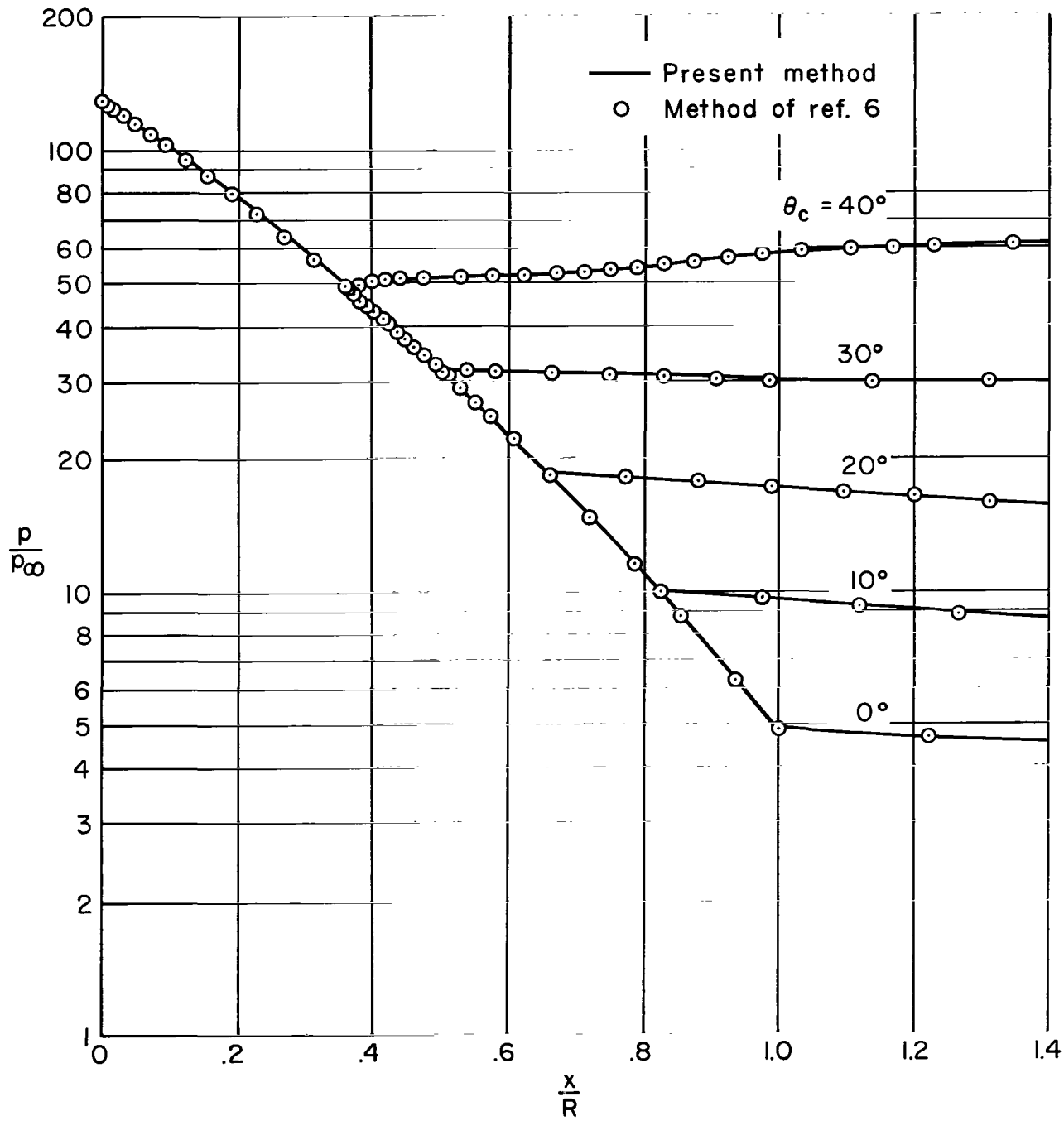

(c) $M_\infty = 10$

Figure 5.- Concluded.

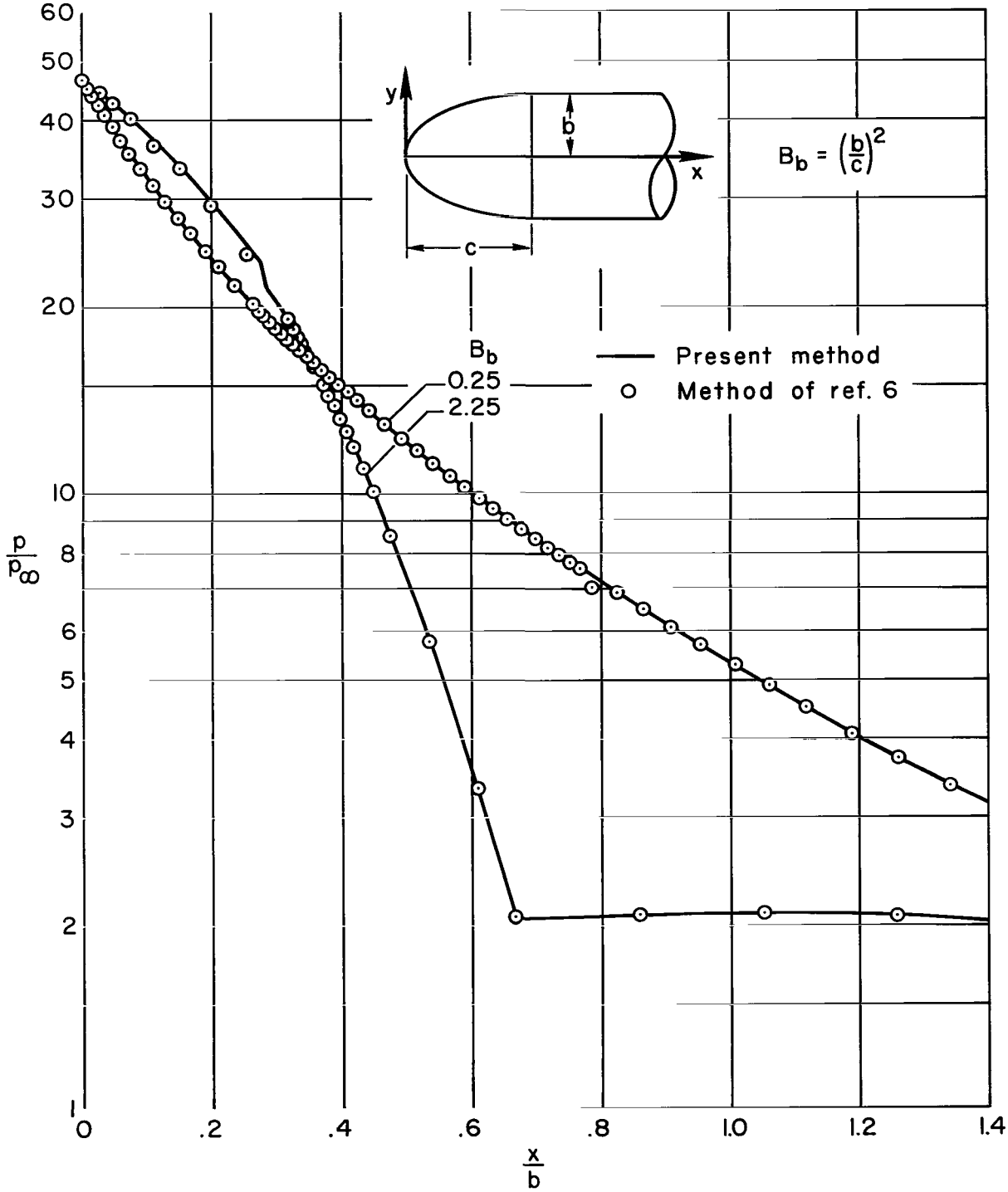

Figure 6.- Surface-pressure distribution on ellipsoid cylinder; $\gamma = 1.4$, $M_\infty = 6$.

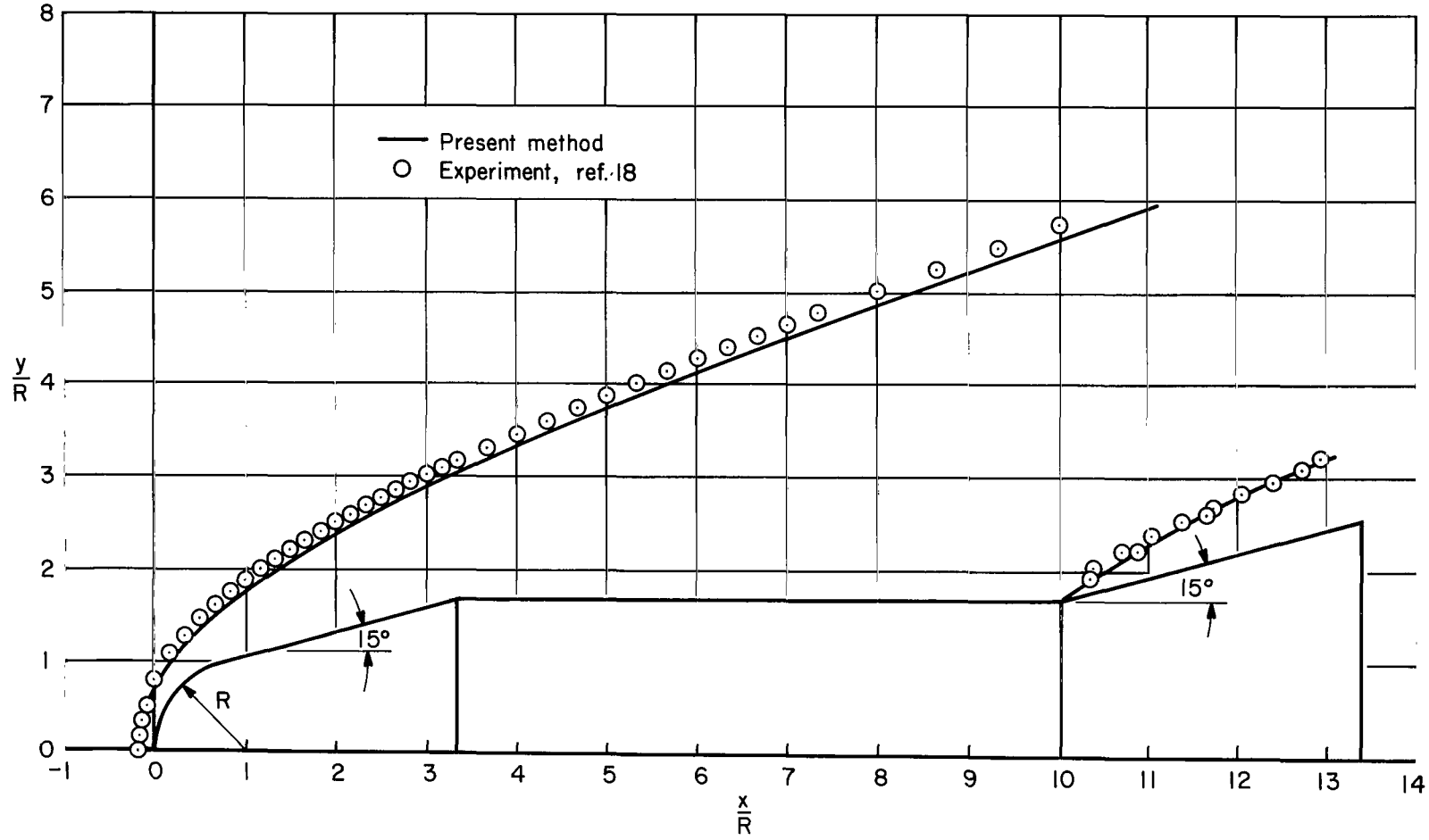

Figure 7.- Comparison of theoretical and experimental shock-wave shapes for a flared body; $\gamma = 1.4$, $M_\infty = 4.1$.

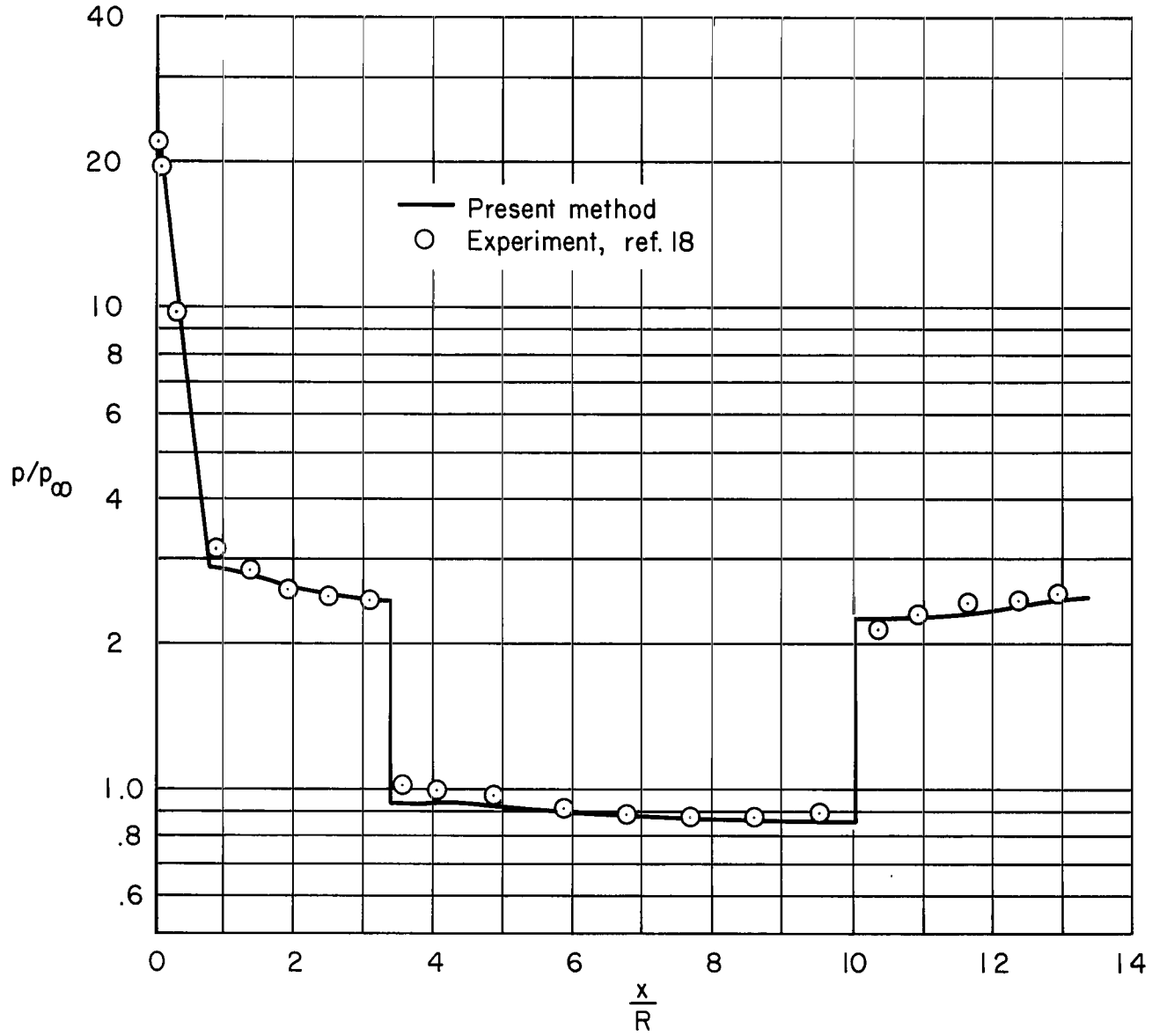

Figure 8.- Comparison of theoretical and experimental surface pressures for the flared body of figure 7; $\gamma = 1.4$, $M_\infty = 4.1$.

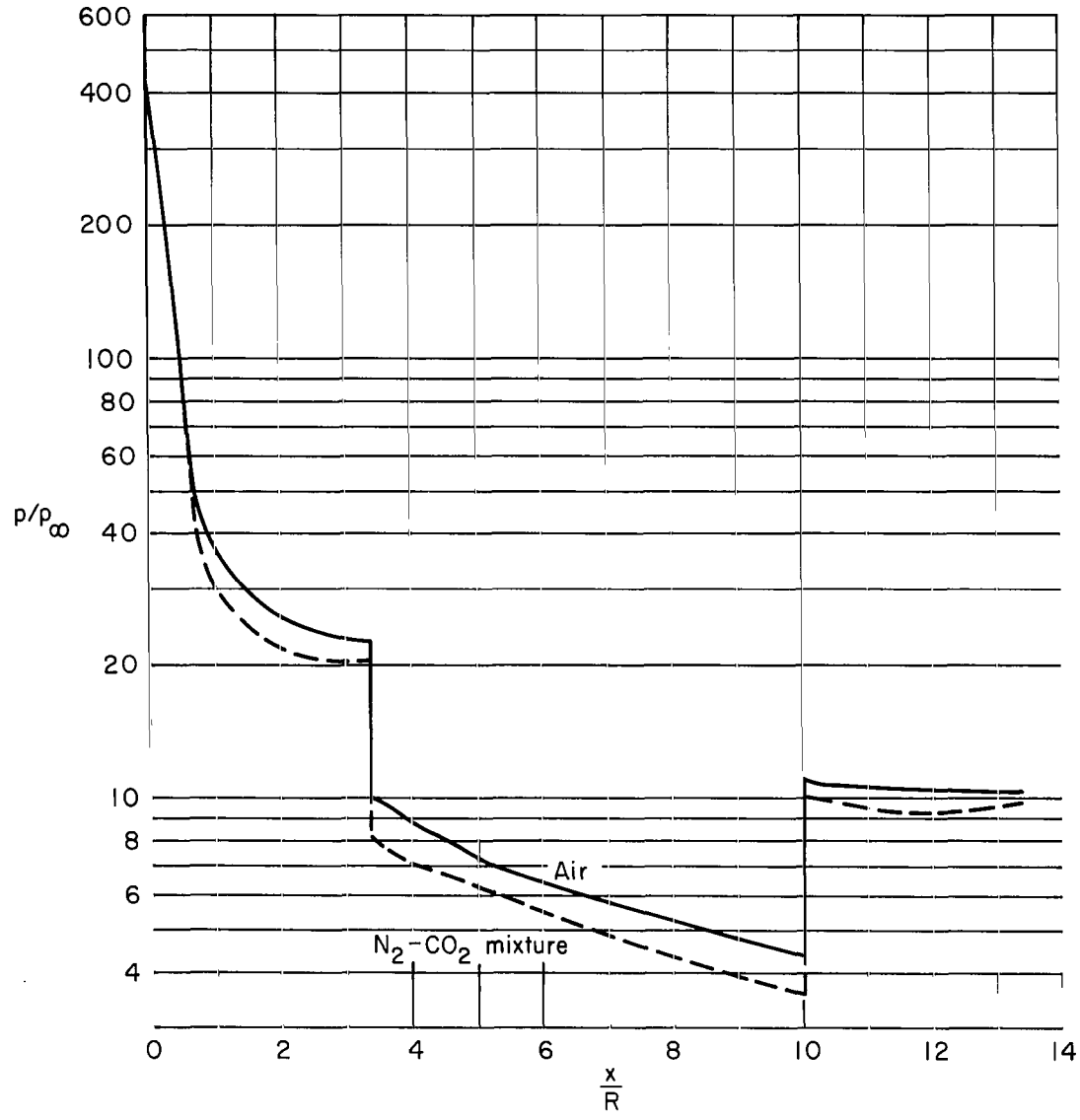

Figure 9.- Comparison of surface-pressure distributions on flared body of figure 7 for air and for a mixture composed of 51.2 percent N_2, 48.8 percent CO_2; V_∞ = 6.10 km/sec, ρ_∞ = 1.225 g/m^3, p_∞ = 101.2 N/m^2.

"The aeronautical and space activities of the United States shall be conducted so as to contribute . . . to the expansion of human knowledge of phenomena in the atmosphere and space. The Administration shall provide for the widest practicable and appropriate dissemination of information concerning its activities and the results thereof."

—NATIONAL AERONAUTICS AND SPACE ACT OF 1958

NASA SCIENTIFIC AND TECHNICAL PUBLICATIONS

TECHNICAL REPORTS: Scientific and technical information considered important, complete, and a lasting contribution to existing knowledge.

TECHNICAL NOTES: Information less broad in scope but nevertheless of importance as a contribution to existing knowledge.

TECHNICAL MEMORANDUMS: Information receiving limited distribution because of preliminary data, security classification, or other reasons.

CONTRACTOR REPORTS: Technical information generated in connection with a NASA contract or grant and released under NASA auspices.

TECHNICAL TRANSLATIONS: Information published in a foreign language considered to merit NASA distribution in English.

TECHNICAL REPRINTS: Information derived from NASA activities and initially published in the form of journal articles.

SPECIAL PUBLICATIONS: Information derived from or of value to NASA activities but not necessarily reporting the results of individual NASA-programmed scientific efforts. Publications include conference proceedings, monographs, data compilations, handbooks, sourcebooks, and special bibliographies.

Details on the availability of these publications may be obtained from:

SCIENTIFIC AND TECHNICAL INFORMATION DIVISION

NATIONAL AERONAUTICS AND SPACE ADMINISTRATION

Washington, D.C. 20546